Hindawi
Geofluids
Volume 2019, Article ID 2453786, 14 pages
https://doi.org/10.1155/2019/2453786

Research Article

The Role of Initial Soil Conditions in Shallow Landslide Triggering: Insights from Physically Based Approaches

L. Schilirò, G. Poueme Djueyep, C. Esposito, and G. Scarascia Mugnozza

Department of Earth Sciences and Research Center for the Geological Risks (CERI), "Sapienza" University of Rome, Piazzale Aldo Moro 5, 00185 Rome, Italy

Correspondence should be addressed to L. Schilirò; luca.schiliro@uniroma1.it

Received 8 March 2019; Accepted 9 May 2019; Published 2 June 2019

Guest Editor: Massimiliano Bordoni

In the last years, the shallow landslide phenomenon has increasingly been investigated through physically based models, which try to extend over large-area simplified slope stability analyses using physical and mechanical parameters of the involved material. However, the parameterization of such models is usually challenging even at the slope scale, due to the numerous parameters involved in the failure mechanism. In particular, considering the scale of the phenomenon, the role of transient hydrology is essential. For this reason, in this work we present the outcome of different experimental tests conducted on a soil slope model with a sloping flume. The tested material was sampled on Monte Mario Hill (Rome, Central Italy), an area which has been frequently affected by rainfall-induced landslide events in the past. In this respect, we also performed a physically based numerical analysis at the field conditions, in order to evaluate the response of the terrain to a recent extreme rainfall event. The results of the flume tests show that, for the same material, two different triggering mechanisms (i.e., uprise of a temporary water table and advance of the wetting front) occur by varying the initial water content only. At the same time, the results of the numerical simulations indicate that clayey sand and lean clay are the soil types mostly influenced by the abovementioned rainfall event, since the initial moisture conditions enhance the formation of a wide wetting front within the soil profile.

1. Introduction

Many of the rainfall-induced landslides occurring all over the world are shallow-type; namely, the sliding surface is located at a depth from a few decimeters to some meters. They generally occur in response to prolonged intense rainfall events and involve either residual weathered soils or transported colluvial deposits. This type of landslides represents a widespread hazard that frequently results in considerable damage to infrastructure and human losses in many mountainous regions of the world, especially in areas characterized by the widespread presence of natural (e.g., [1–3]) and/or human-reworked soil cover (e.g., [4–6]). For this reason, in recent years great efforts are being made to improve the assessment of the temporal and spatial occurrence of rainfall-induced shallow landslides, especially through physically based models (e.g., [7–10]). However, the fundamental controls leading to slope failure driven by rainfall are still not well quantified [11], and thus the improvement of current models is still an important research topic [12]. In fact, despite the small size, it is not straightforward to define the complex interaction between hydrological and mechanical processes that develops before and during the triggering process [13]. In principle, the infiltrating water flow may cause both the development of a temporary perched water table, usually at the contact between the soil cover and the less permeable bedrock [14], and a decrease of the resisting effect (apparent cohesion) induced by increasing positive water pressure values in the unsaturated portion [15, 16]. In this respect, it has been well recognized that matric suction can play a crucial role in the stability of unsaturated soil slopes [17]. Additionally, rainfall-induced slope failures heavily depend on the relationship between suction and water content which, in turn, are related with unsaturated conductivity functions as well as the rainfall intensity [18]. Considering the complexity of this research topic, a considerable amount of experiments has been conducted on understanding the behavior of water-induced shallow landslides under controlled laboratory

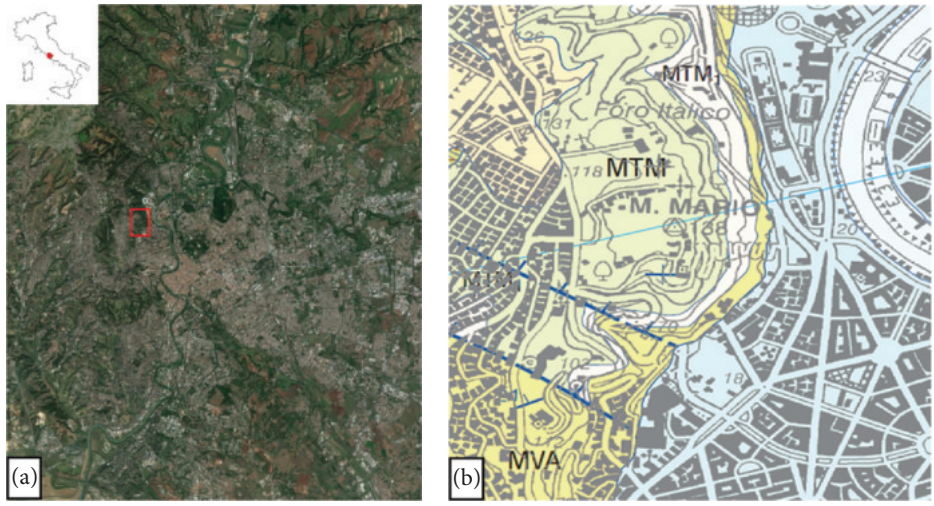

(a) (b)

Figure 1: (a) Satellite image of the Rome urban area, with the location of Monte Mario Hill; (b) geological sketch of the Monte Mario area (from [36]).

conditions using sloping flumes (e.g., [19–23]). Several authors [24–26] also reproduced via numerical modelling the performed experimental tests, assuming a triggering mechanism that commonly occurs when the wetting bands progress into the soil, resulting in loss of suction and in effective stress reduction [27, 28]. Although these studies significantly contributed to better understanding the conditions leading to water-induced shallow landslides, there have been relatively few investigations for linking such experimental evidences with real widespread landslide events [29], evaluating in detail the triggering mechanisms [30]. In this sense, physically based models aimed at predicting the occurrence of shallow landslides over large areas (e.g., [31–34]) can be viewed as reliable tools, unless the uncertainties concerning the input parameter values be reduced as much as possible.

For this reason, in this work we analyze the triggering mechanisms of shallow landslides evaluating the effect of the initial soil conditions through laboratory flume experiments. Specifically, different tests have been performed on a soil sampled on Monte Mario Hill (Rome, Central Italy). This area has been affected by recurring rainfall-induced landslide events in the past, including the one that occurred between January 31 and February 2, 2014. In this sense, the outcome of the experiments has been also analyzed in relation to the results provided by HYDRUS-1D [35], a USDA (United States Department of Agriculture) Salinity Laboratory software package which can simulate the water flow into unsaturated porous media resulting from a rainfall event. Specifically, the insights resulting from the laboratory tests and the numerical simulations have been used to better understand the potential failure conditions for the shallow landslides occurred during the 2014 event.

2. General Features of the Study Area and the 2014 Event

The Monte Mario Hill, which is located in the northwestern sector of the city of Rome, on the right bank of Tiber River (Figure 1(a)), represents the highest relief of the city (144 m a.s.l.). From a geological point of view (Figure 1(b)), it is composed at the bottom by a silty-clay succession of lower-upper Pliocene age (Monte Vaticano Formation (MVA)). This formation has a discordant contact with the upper Monte Mario Formation (MTM), a lower Pleistocene succession composed of silty sands [37]. At the base of this formation, it is also possible to identify a portion of reduced thickness (15 m) constituted by clayey silts (Farneto Member MTM_1). From a morphological point of view, Monte Mario is characterized by a relatively high slope gradient, especially along the eastern sector, which represents the result of both natural and anthropogenic factors, like fluvial erosion and manmade cuts. Such a slope gradient also enhances the triggering of rainfall-induced landslides, which generally involve a thin (0.5–2 m) layer of eluvial-colluvial superficial deposits overlaying the majority of the slopes. In this respect, between January 31 and February 2, 2014, 68 landslides have been recorded all around the city (Figure 2(a)), of which 12 occurred along slopes of Monte Mario only [38]. According to the data recorded by the Roma Monte Mario station, which is located within the study area, such landslides have been triggered by approximately 250 mm of rainfall cumulated in three days. However, in this time interval, two main subevents may be distinguished. The first (and most severe in terms of rainfall amounts) started in the early hours of January 31st and ended after about 24 hours, with a total cumulated rainfall of about 190 mm. This subevent was characterized by extremely high rainfall intensity peaks, such as the one that occurred between 4:00 and 5:00 a.m. (46 mm). Very high values continued to be recorded throughout the morning, with 3-hour and 6-hour rainfall equal to 87.6 and 140 mm, respectively. On the contrary, the second subevent, which took place in the afternoon of February 2nd from about 1:00 to 6:00 p.m., was of shorter duration and characterized by less intensity peaks, resulting in a total average cumulated rainfall of approximately 40 mm. Most of the triggered landslides involved relatively shallow (less than 1 m) portions of

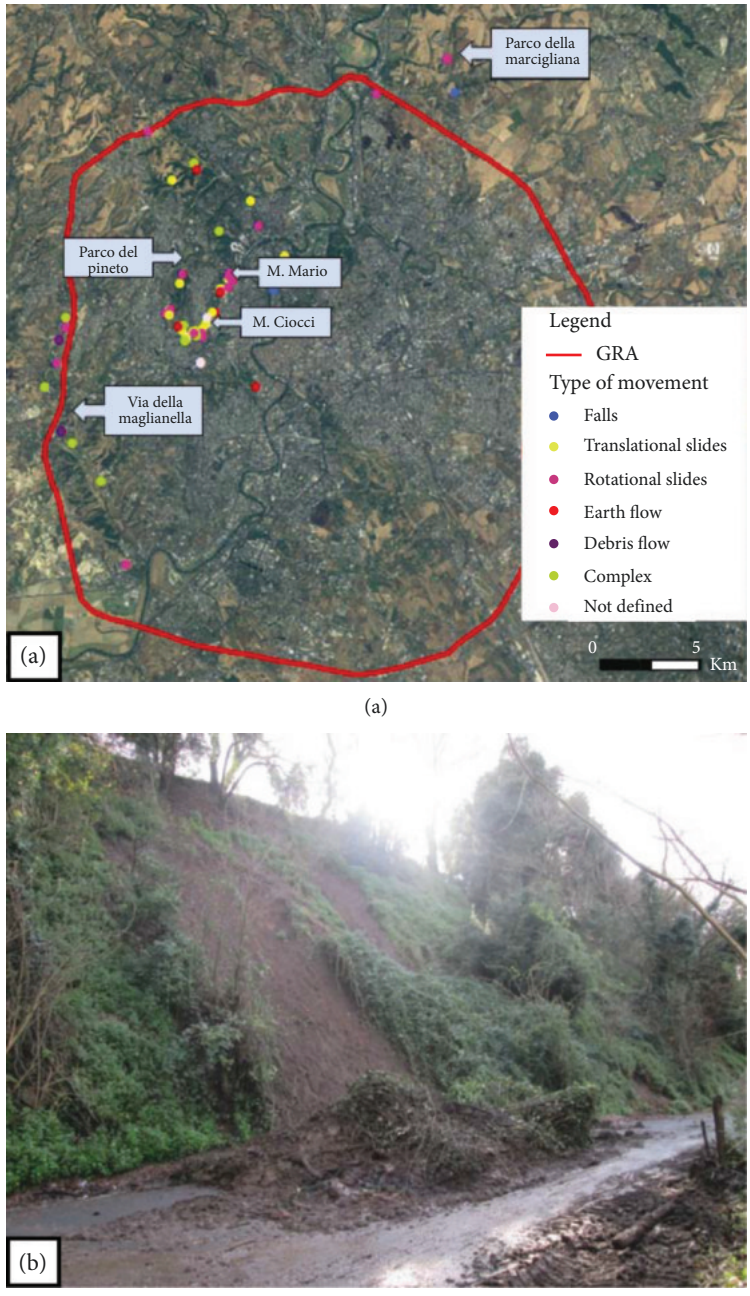

(a)

(b)

Figure 2: (a) Location of landslides inventoried in the Rome urban area after the exceptional rainfall of January 31-February 2, 2014 (from [38]); (b) an example of landslide triggered on Monte Mario Hill during the 2014 event.

weathered soil (Figure 2(b)) and can be classified as translational and rotational slides, earth flows, and debris flows [38]. Despite their limited thickness, such landslides caused the disruption of the road network, with consequent vehicle traffic bans and inconveniences for citizens as well as substantial damages to other infrastructures.

3. Materials and Methods

3.1. Physical and Mechanical Characterization of the Soil Cover. A series of field and laboratory activities have been carried out in order to outline the main features of the soil cover affected by the slope failures that occurred in 2014. After removing the most surficial soil layer (approximately 20 cm), twenty-one undisturbed samples have been collected on site by driving into the soil a core cutter having a diameter of 100 mm (Figures 3(a) and 3(b)). The material is generally characterized by a medium plasticity and a high content of sand and clay, while the gravel and silt amount seldom exceeds 20-30% (Table 1). Specifically, the sampled material can be identified in four different USCS classes, which are consistent with eluvial and colluvial deposits resulting from

(a)

(b)

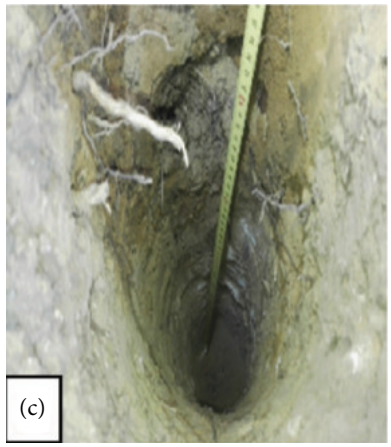

(c)

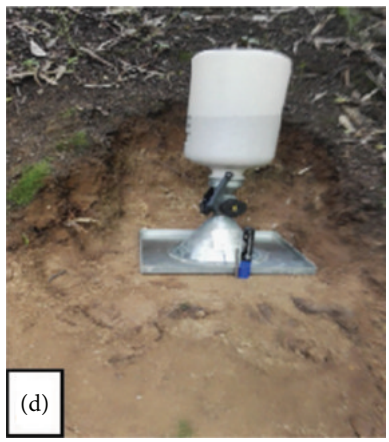

(d)

Figure 3: (a) Locations of the 21 samples collected on Monte Mario; (b) the sampling stage; (c) borehole for the evaluation of the soil cover thickness. The location of the three boreholes is marked in green in Figure (a); (d) test for density and unit weight of soil in place by the sand cone method.

Table 1: Physical properties and corresponding USCS-USDA class for the 21 samples collected on Monte Mario Hill.

Sample code	Soil thickness (m)	Gravel (%)	Sand (%)	Silt (%)	Clay (%)	W_L (%)	IP (%)	USCS class	USDA class
S1		22.3	33.9	16.7	27.1	29	5.7	SC	Loam
S2		4.2	12.7	34.5	48.6	39.6	11.6	CL	Silty clay loam
S3		19.6	52	13	15.4	—	—	SC	Sandy loam
S4		25.3	50.8	12.8	11.1	—	—	SM	Sandy loam
S5		5.5	66.4	8.6	19.5	25.9	4.8	SC	Sandy loam
S6	1.3	4	51	17.1	27.9	36.2	10.7	SC	Sandy clay loam
S7		8.4	77.5	0.9	13.2	—	—	SC	Loamy sand
S8		6.5	87.5	3	3	—	—	SM	Sand
S9		2.8	9.6	36.5	51.1	35.1	11.3	CL	Clay loam
S10		9.1	19	30.2	41.7	34	9.8	CL	Clay loam
S11		6.4	63.8	11.4	18.4	—	—	SC	Sandy loam
S12		13.3	68.3	11.5	6.9	—	—	SM	Loamy sand
S13	1.1	0	3.8	38.5	57.7	50.3	16	MH	Silty clay
S14		7	35.6	29.5	27.9	25.2	6.1	CL	Loam
S15		5.4	25.3	29.8	39.5	37.9	14.6	CL	Clay loam
S16		16.1	30.7	24	29.2	29.8	8.5	CL	Loam
S17		1.1	13.6	35	50.3	45.4	10.8	CL	Silty clay loam
S18		0	3.5	50.2	46.3	32.9	5.7	CL	Silty clay loam
S19		1	7	27.5	64.5	48.6	15.3	CL	Silty clay
S20	0.75	5.7	30.3	21.3	42.7	41.9	16.8	CL	Clay loam
S21		10.7	48.6	13.9	26.8	34.2	11.5	SC	Sand

the weathering of medium to fine-grained rocks, such as those outcropping on Monte Mario Hill. In this respect, the sandy samples have been mainly collected where the Monte Mario Formation outcrops (i.e., medium-upper part of the slope), while the material characterized by a higher amount of clay was generally sampled in the lower part of the slope, in correspondence of the Monte Vaticano Formation.

In correspondence of sampling site S21, further material (approximately 500 kg) has been collected for performing the flume tests described in Section 3.2. In this sense, it is important to specify that the soil unit weight has been determined in this specific site by the sand cone method (Figure 3(d)), and the resulting value (14.9 kN/m^3, which corresponds to a porosity of 48%, given a unit weight of soil solids of 26.4 kN/m^3 and a field water content of 11.5%) has been properly reproduced within the flume during the experimental tests.

3.2. Experimental Set-Up. The experimental equipment (Figure 4(a)) comprises a rectangular sloping flume 100 cm long, 60 cm wide, and 20 cm high, whose sides were made in plexiglass in order to allow the visual observation of the wetting and triggering processes. To assure the same friction between the soil particles and the base of the flume as of that of particles inside the flume, a rough plastic panel was applied to the surface of the flume base. A stiff permeable barrier was fixed in front of the soil to contain it after the failure, whereas a video camera was used to monitor failure initiation time and location. Two properly placed spray nozzles above the flume guarantee an artificial rainfall having a raindrop size distribution and impact energy consistent with the experiment scale (Figure 4(b)). For assuring the correct functioning of the system, the supplied water pressure has been kept constant at 3.2 bar, resulting in a steady rainfall input of approximately 1/mm/min. During each test, the water content and pore water pressure within the soil were measured using, respectively, 4 EC-5 soil moisture sensors and 4 UMS-T5 mini-tensiometers (Figure 4(c)). These sensors are connected to a data logger which acquires data each two seconds.

Three different flume inclinations have been used during the experiments (i.e., 27°, 32°, and 35°) which represent, respectively, the minimum, average, and maximum slope values within the 2014 landslide source areas. The soil initial water content ranges between 11.9% and 19.2%, and it was obtained, before placing the soil into the flume, by wetting a specific quantity of oven-dried soil with the amount of water needed to reach the desired water content value. After the soil was set into the flume, the water content was checked by sampling the soil in different points. The initial porosity was attained overlaying four compacted soil layers parallel to the flume base (Figure 5(a)). Given the fixed geometry and volume of a 4 cm thick layer, the soil weight required to fill that volume was calculated considering also the fixed initial water content. During the soil placement within the flume, the 8 sensors have been placed at different depths (Figure 5(b)), with the aim of observing the infiltration process throughout the soil slope model. Finally, in order to achieve the least possible disturbance of slope conditions, a wedge-shaped slope was created in the termination of the material (Figure 5(c)). The inclination of the wedge-shaped

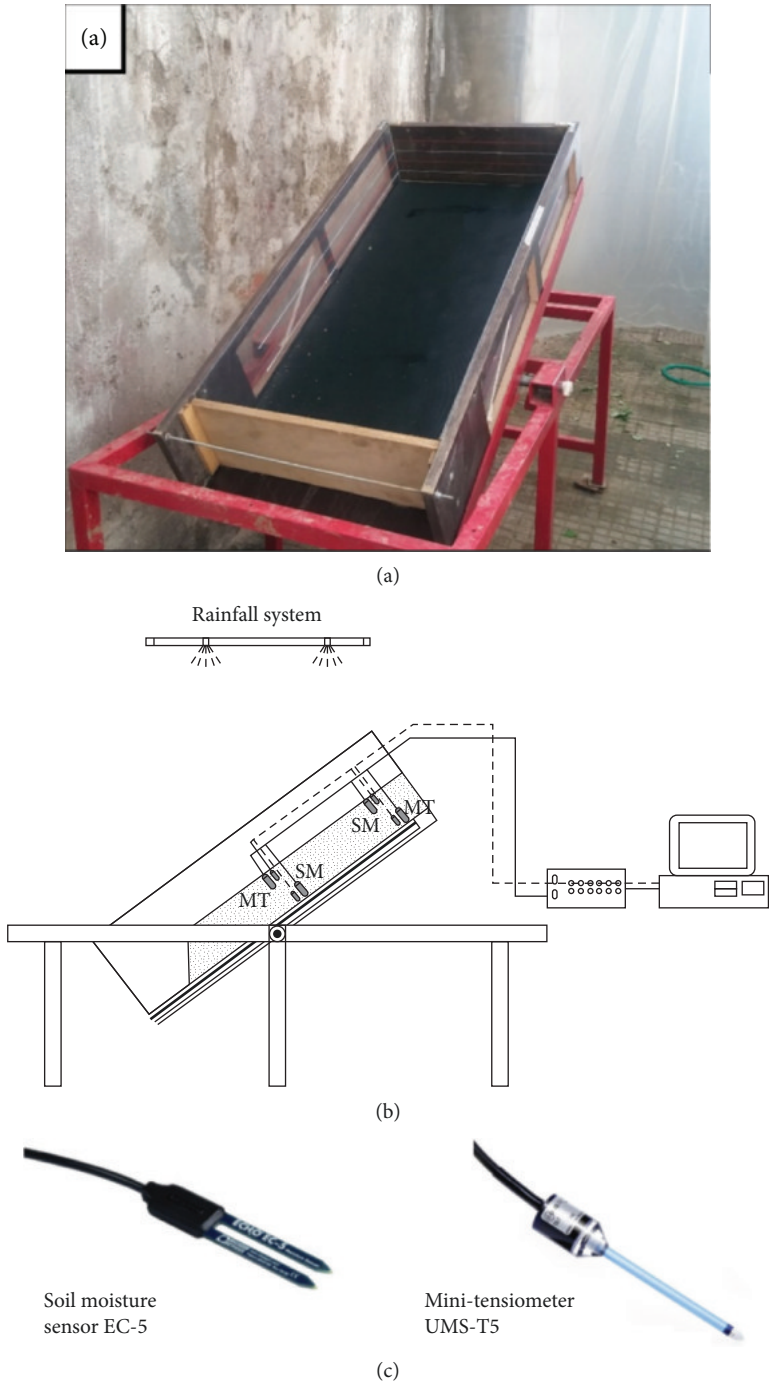

Figure 4: (a) The experimental flume; (b) scheme of the experimental apparatus (SM: soil moisture sensor; MT: mini-tensiometer); (c) sensors used for the monitoring of soil water content and pore water pressure during the tests.

slope was set to 30° (lower than the friction angle) to ensure that failure occurred within the soil volume and not affecting this terminal slope only. This geometry was considered suitable for the experimental purposes, and then, it has been kept constant in each test.

4. Results

Ten flume tests have been performed by varying the initial water content (w) and the flume slope angle (α) (Table 2). According to the obtained results, different observations can be made: (1) as the initial water content or slope increases, the failure time decreases (Figure 6); (2) by changing the initial water content, the failure time variation is higher in tests with a slope angle (α) of 35° than in those with 32° (Figure 6); (3) in tests with $\alpha = 27°$, no failure occurred, but only a gradual erosion of the superficial layers, even with the wettest initial soil conditions (i.e., $w = 16.4\%$); (4) tests n.9 and n.10 have been performed for replicating tests n.6 and n.3, respectively. The aim was to evaluate the

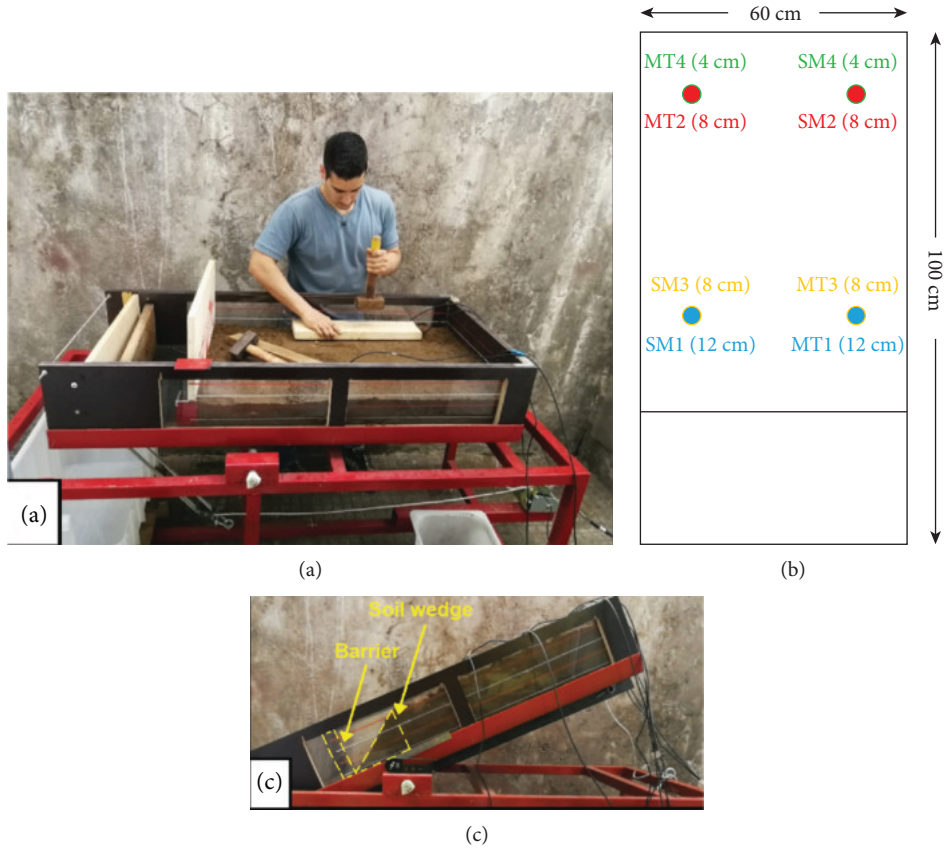

Figure 5: (a) Placement of a 4 cm soil layer within the flume; (b) position and installation depth of the 8 sensors according to a schematic upper view of the soil slope model; (c) the soil slope model just before the beginning of a test. The lateral view allows to notice the wedge-shaped slope at the termination of soil volume.

Table 2: Initial soil conditions and time of failure for each performed flume test.

Test	Date	Slope angle (°)	Initial water content (%)	Degree of saturation (%)	Time of failure (min)
1	24/04/2018	27	12.4	36.1	No failure
2	29/04/2018	27	16.4	47.8	No failure
3	09/05/2018	32	11.9	34.7	1 h 21 min 05 sec.
4	15/05/2018	32	14.7	42.8	1 h 13 min 50 sec.
5	25/05/2018	32	19.2	56.0	0 h 45 min 00 sec.
6	04/06/2018	35	11.9	34.7	0 h 42 min 08 sec.
7	11/06/2018	35	14.4	42.0	0 h 37 min 30 sec.
8	14/06/2018	35	16	46.6	0 h 24 min 37 sec.
9	05/07/2018	35	12.1	35.3	0 h 45 min 47 sec.
10	18/07/2018	32	12.0	35.0	1 h 25 min 45 sec.

reproducibility of the assumed boundary conditions and, in turn, the reliability of the obtained results: in both tests, the failure time difference with the corresponding tests is lower than five minutes.

As regards the failure mode, it was generally extremely rapid, with evidences of incipient instability only a few seconds before the failure (Figure 7). The detachment generally involved a soil thickness between 7 and 12 cm; thus, considering that the total soil thickness is 16 cm, the failure surface always developed within the soil profile and not at the contact between soil and the flume base. Furthermore, it is worth noting that, if the initial water content is relatively low, failure typically induces the mobilization of greater soil volumes, and vice versa.

Other interesting observations can be made by analyzing the records from the eight sensors placed within the soil during the tests. In this respect, if we compare data from test n.3 ($\alpha = 32°$, $w = 11.9\%$) and test n.5 ($\alpha = 32°$, $w = 19.2\%$), a different soil behavior in response to the rainfall input can be recognized. Specifically, in both tests

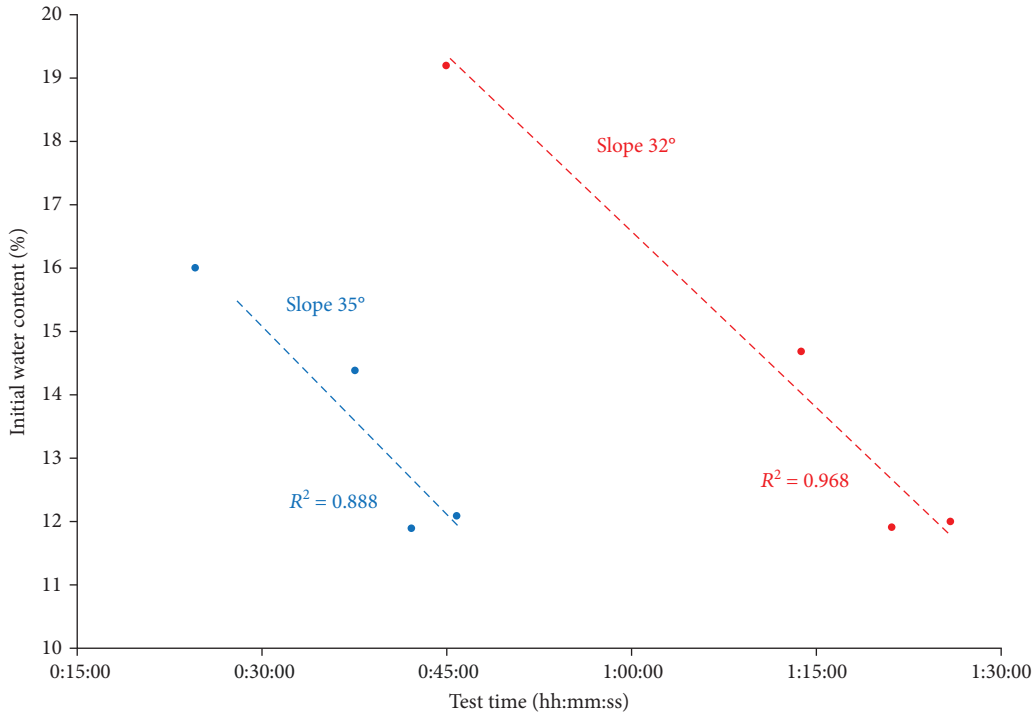

Figure 6: Failure time vs. initial water content for different flume slopes.

starting from initial negative values of pore water pressure induced by partial soil saturation, soil undergoes progressive reduction of the matric suction, until the development of positive pore water pressures. However, in test n.3 such development occurs first for the deepest mini-tensiometers (MT1 and MT2) and then for the shallowest ones (MT3 and MT4) (Figure 8(a)). On the contrary, in test n.5, the sensors that first record a drastic reduction of matric suction are those located in the most surficial portion of soil (Figure 8(b)). Actually, in this specific test also MT2 recorded positive pore water pressures almost simultaneously to MT3; however, this point can be explained with a not sufficient soil compaction in the area above the sensor, which caused an excessive water percolation in that specific point.

As regards the water content, even if in test n.3 the first sensor that records an increase in water content is the shallowest one (SM4), at the end of the test the highest values are still recorded by the deepest sensors (SM1 and SM2) (Figure 8(c)). Conversely, in test n.5, SM3 and SM4 first recorded an increase in water content, reaching the highest values during the whole test (Figure 8(d)).

The same behavior, in terms of infiltration, can be observed also in tests with $\alpha = 35°$ (Figure 9). In such a case, the greater slope angle induces most sudden variations of water content and pore water pressure, also enhancing an earlier response of sensors located closer to the soil wedge (i.e., MT1-MT3, and SM1-SM3). In this respect, it is worth noticing that in test n.6 ($w = 11.9\%$) failure occurs while the sensors farthest from the soil wedge (MT4 and MT2) still recorded negative pore water pressure values (Figure 9(a)).

5. Discussions

On the basis of the observations deriving from the outcomes of the performed tests, different insights can be inferred. Firstly, a strong sensitivity of the tested material to changing the flume slope angle can be noticed. In fact, if no failure was observed for $\alpha = 27°$ regardless of the rainfall duration, for tests with $\alpha = 32°$, failure occurred in about one hour, and the time of failure strongly reduces, increasing by just three degrees the flume slope. Afterwards, a different response of the soil, in terms of infiltration, was observed by varying the initial water content, while keeping constant both slope and porosity, as well as the rainfall input. Specifically, for tests with lower initial water content, the sensors that first recorded variations induced by the infiltrating water flux are those located in the deepest part of the soil. On the contrary, for tests with higher initial water content, the first variations were detected by the shallowest sensors. This point suggests two different triggering mechanisms for the soil slope model. In the first case, it is possible to hypothesize the formation of a temporary water table at the base of the flume, which progressively rises until failure occurs, involving a relatively high amount of material (Figure 10(a)). In the second case, failure is likely induced by the advance of the wetting front, which mobilizes a lower soil thickness with respect to the preceding instance (Figure 10(b)). Therefore, the most interesting insight deriving from the flume tests is that the triggering mechanism may change only considering variation of the initial water content. In preceding works, several authors (e.g., [39–41]) highlight how antecedent soil moisture greatly affects the rate and depth of advance of the wetting front during intense rainfall, but not the type of

Figure 7: Temporal evolution of failure during test n.3.

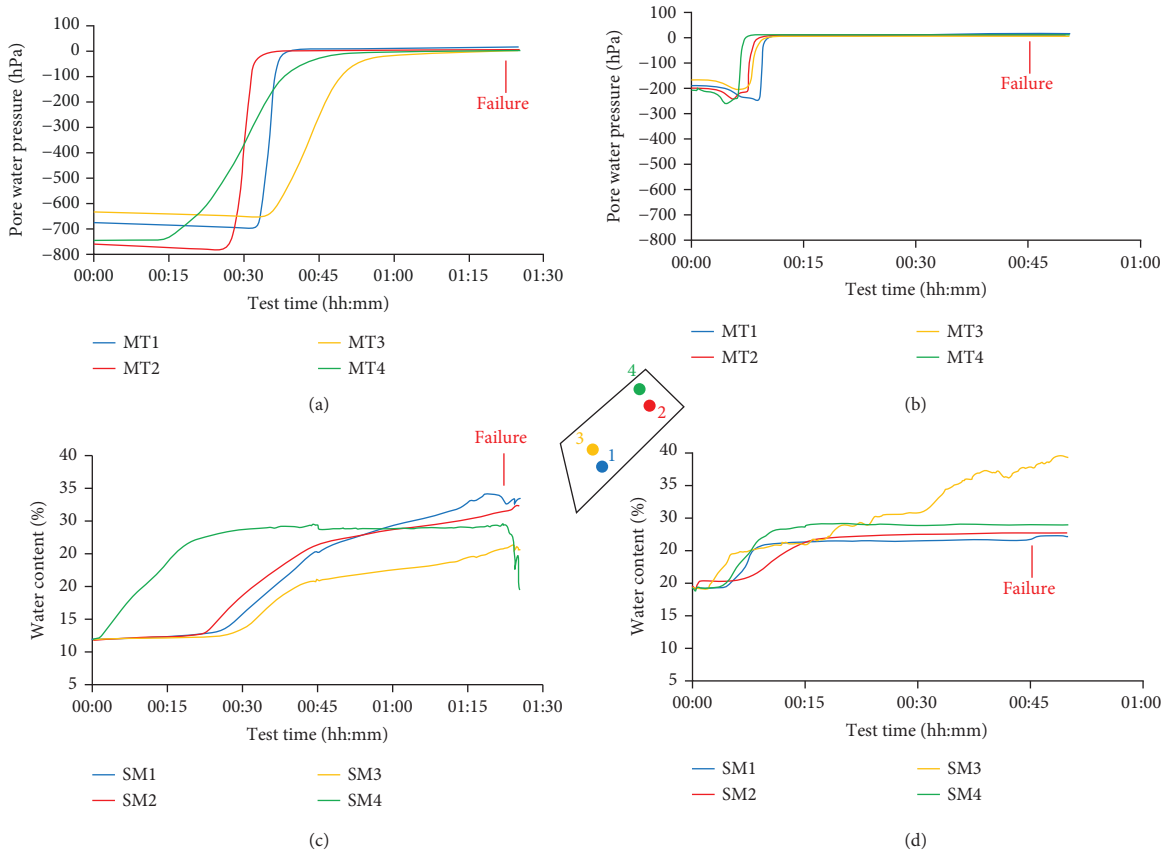

Figure 8: Pore water pressure (a and b) and soil moisture data (c and d) recorded during test n.3 ($\alpha = 32°$, $w = 11.9\%$) and test n.5 ($\alpha = 32°$, $w = 19.2\%$), respectively.

triggering mechanism that, instead, is generally associated with the rainfall intensity [28, 42] and grain-size soil characteristics. In this sense, [43] assert that shallow landslides affecting fine-grained soils are induced by the reduction in matric suction near the ground surface due to rainfall infiltration, while a significant triggering factor for coarse-grained soils of high permeability like sands is a rise in the water table.

Therefore, the role of initial soil moisture in relation to the triggering mechanism should be examined more in detail for evaluating the potential shallow landslide triggering conditions, especially when physically based numerical models are employed. In this respect, it is considered that one of the main drawbacks of such models relies on the complexity in correctly evaluating the input parameters, especially over large areas. In this respect, different authors (e.g., [44–46])

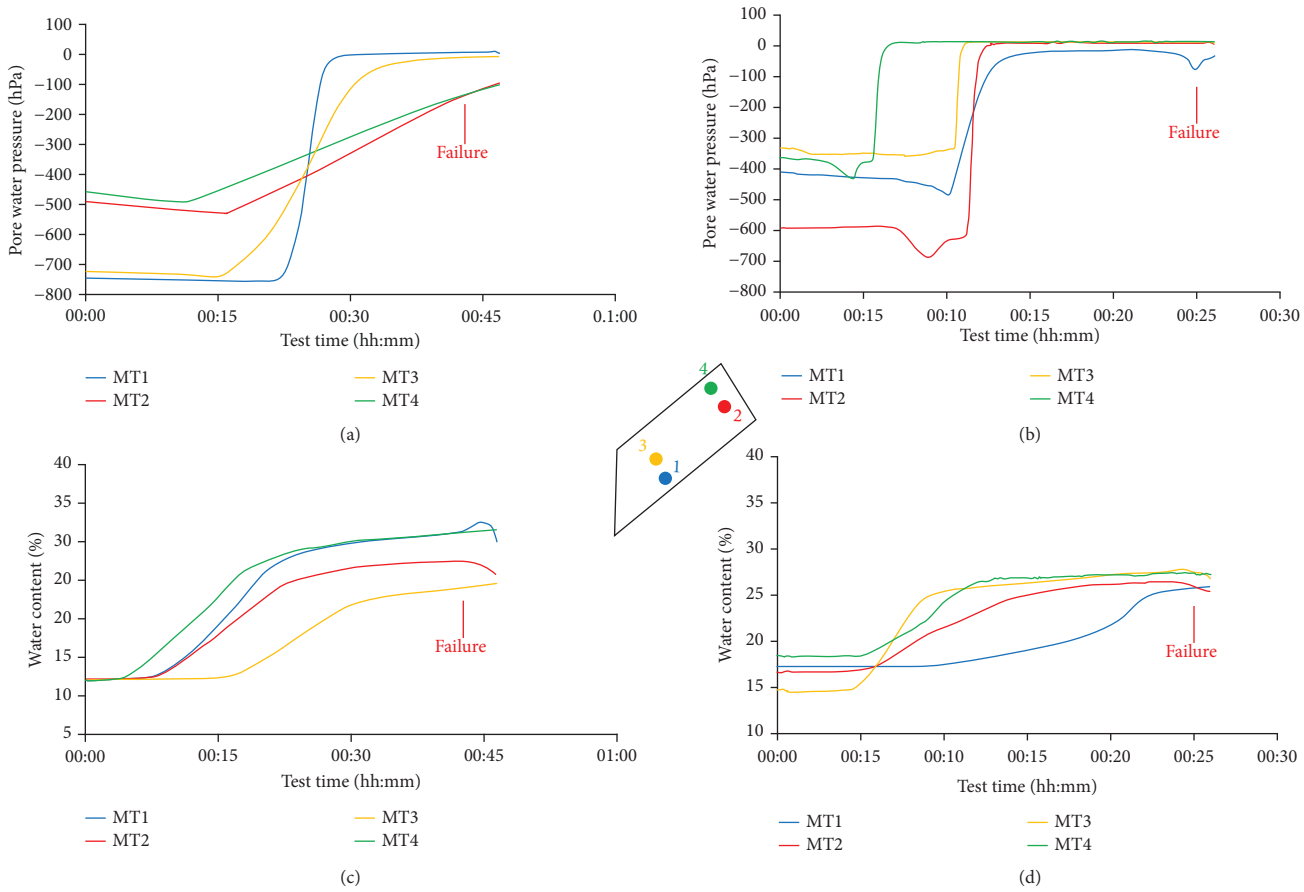

Figure 9: Pore water pressure (a and b) and soil moisture data (c and d) recorded during test n.6 ($\alpha = 35°$, $w = 11.9\%$) and test n.8 ($\alpha = 35°$, $w = 16\%$), respectively.

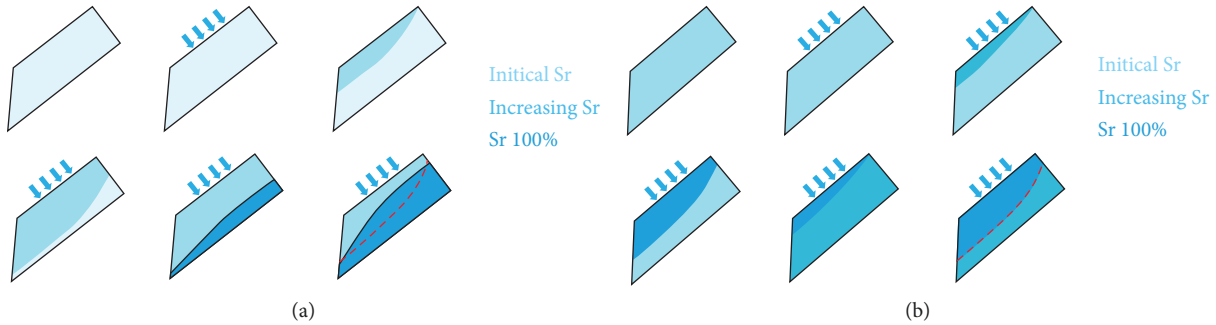

Figure 10: The triggering mechanisms hypothesized according to the experimental evidences: (a) failure induced by an uprise of a temporary perched water table (for soils with relatively low initial water content); (b) failure induced by the advance of the wetting front (for soils with relatively high initial water content).

have observed that soil cohesion, friction angle, and soil thickness represent the major sources of error for this type of analyses. With regard to the mechanical parameters, the problem is mainly related to the limited sampling [47, 48] and the difficulty to properly evaluate the vegetation effect in terms of root cohesion [49, 50]. As regards the soil thickness, several authors proposed linear correlations with elevation and slope gradient [51], semi-empirical geomorphology-based approaches [52], and multivariate statistical analyses of terrain parameters [53]. However, the results of the experimental tests demonstrate that a reliable analysis of the

Table 3: Hydrodynamic parameters for the four soil types of Monte Mario (θ_r: residual water content; θ_s: saturated water content; K_s: hydraulic conductivity).

Soil type	θ_r (-)	θ_s (-)	K_s (m s^{-1})
SC	0.06	0.39	$3.84E-06$
CL	0.07	0.37	$3.41E-07$
MH	0.08	0.36	$1.14E-07$
SM	0.04	0.35	$1.53E-05$

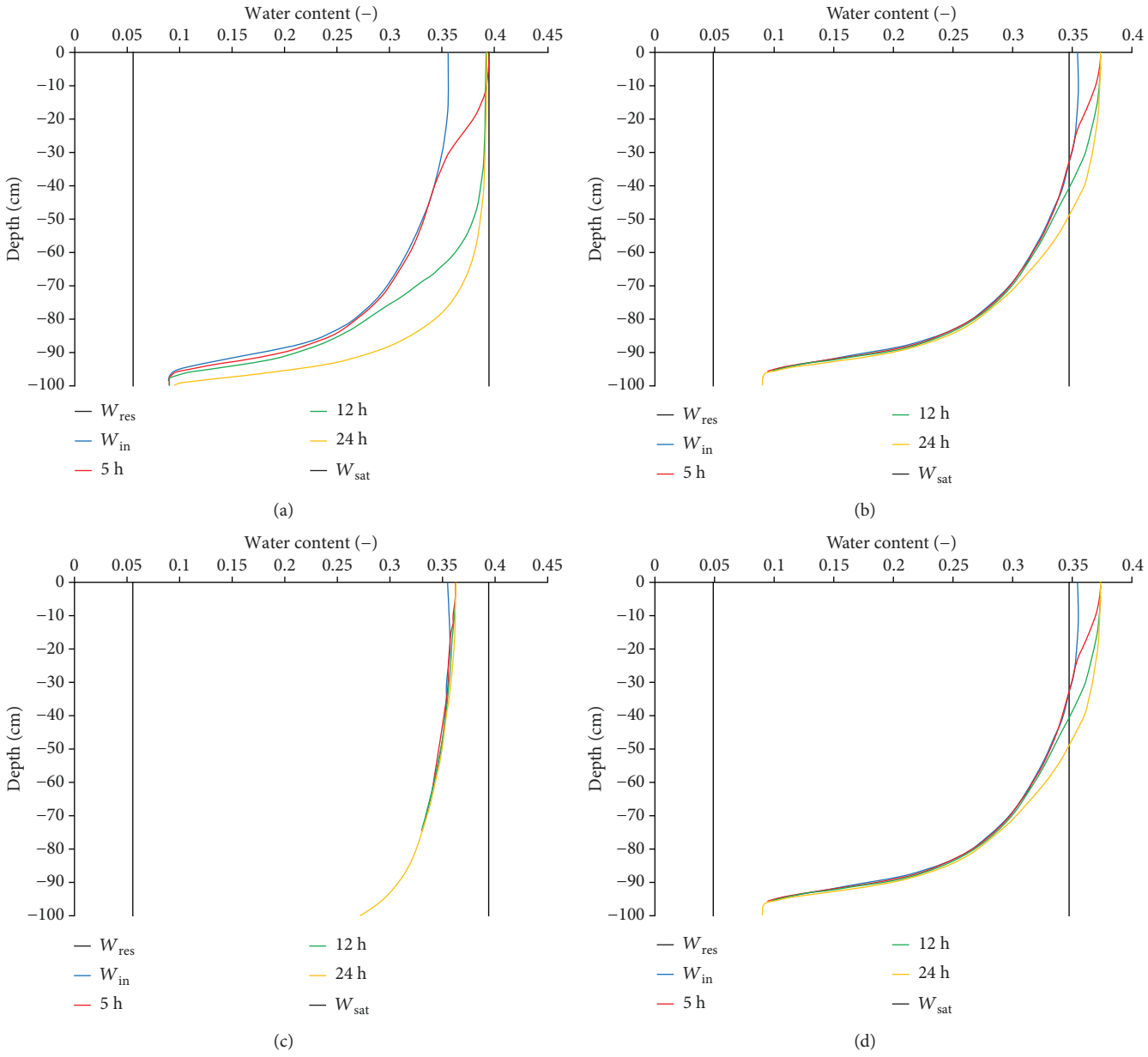

Figure 11: Water content trend vs. depth resulting from the HYDRUS-1D simulation of the January 31-February 1, 2014, rainfall event that occurred in Rome. Each graph refers to one of the soil types outcropping on Monte Mario Hill: (a) clayey sand (SC); (b) lean clay (CL); (c) silt (MH); (d) silty sand (SM). Legend: W_{res}: residual water content; W_{in}: initial water content; W_{sat}: saturated water content.

shallow landslide triggering conditions requires not only the proper evaluation of the input parameters but also the use of an infiltration model that must be coherent with the real expected events.

For this reason, we decided to evaluate the hydraulic effects induced by the rainfall event that occurred in Rome in 2014 to four different soil types outcropping on Monte Mario. To do this, we used HYDRUS-1D, a numerical model which can describe the water flow within an unsaturated porous medium, such as a superficial deposit, on the basis of a modified version of Richards' equation. Different numerical simulations have been first performed for the period August 1, 2013, January 30, 2014, in order to quantify the effect of the antecedent rainfall on soil moisture conditions. Afterwards, the simulations have been extended to include the main rainfall event causing the triggering of the majority of landslides (specifically, between 1 a.m. of January 31st and 1 a.m. of February 1st). The van Genuchten–Mualem model [54] was chosen as a hydraulic model to simulate water flow, whereas the hydrodynamic parameters θ_s, θ_r, and K_s (Table 3) are predicted from soil grain size distribution using the ROSETTA Lite module [55]. Daily rainfall data (source: *Centro Funzionale della Protezione Civile della Regione Lazio*—Functional Civil Protection Centre of the Latium Region) have been used as input for the model, whereas evapotranspiration is accounted for by inserting the maximum and minimum temperature values (source: *Servizio Idrografico e Mareografico Nazionale*—National

Hydrographic and Marine Services) recorded during the investigated period into the Hargreaves equation [56]. With regard to the thickness of the model, we decided to use the average value of the three measurements deriving from the boreholes (1 m), while the soil column inclination has been set in order to obtain a superficial slope equal to 32°.

According to the simulations, it results that SC and CL are the soil types mostly influenced by the rainfall event (Figures 11(a) and 11(b)). In detail, both soils start from relatively high initial (W_{in}) moisture conditions (between 25% and 35% in the first 90 cm of soil). Afterwards, a clear wetting front forms, in particular after the 5 h rainfall and advances, causing the saturation of the first 20-30 cm. It is worth noting how such advance is greater in the case of SC as a consequence of the higher hydraulic conductivity. In the case of MH soil (Figure 11(c)), although W_{in} is similar to that of the preceding soils, the rainfall effect is substantially irrelevant, at least in the short term, probably due to the lower hydraulic conductivity that enhances the run-off. The rainfall impact is small also for SM (Figure 11(d)): in this specific case, W_{in} is quite low and homogenous, which coupled with the high hydraulic conductivity of the material, inducing significant water content changes. However, these variations are not still sufficient to form either a wetting front (excluding the very first cm of soil) or a perched water table at the base of the column.

6. Conclusions

In this study, different flume tests have been performed to analyze the triggering process of rainfall-induced shallow landslides, with a specific focus on the role of the initial hydraulic conditions by changing the slope. In detail, it was observed that the increase in the initial water content anticipates the triggering time, particularly in the case of slope = 35°. This point, together with the lack of failure for tests with $\alpha = 27°$, also suggests the marked sensitivity of the tested material to even small slope variations. With regard to the failure mode, the data deriving from the soil moisture and pore water pressure sensors indicate two potential triggering mechanisms to variations of the initial water content, i.e., failure induced by uprise of a temporary perched water table and by the advance of the wetting front in the case of relatively low and relatively high initial soil moisture, respectively. At this point, for analyzing such process at the field conditions, we performed a numerical analysis with HYDRUS-1D, a physically based model which simulates the water flow into unsaturated porous media. On the basis of the data collected on site (i.e., Monte Mario Hill, Rome), we simulated numerically the rainfall event occurring between January 31 and February 1, 2014, which triggered 68 landslides along slopes of Monte Mario and the surrounding areas. According to the simulations, it results that SC and CL soil types are those mostly influenced by the 2014 rainfall event, since the higher initial moisture conditions enhance the formation of a wide wetting front within the soil profile.

In conclusion, the evidence that the triggering mechanism may change only due to variations of the initial water content should be considered also for future research activities regarding the physically based modelling of shallow landslides. Specifically, future improvements may concern a better evaluation of the role of other parameters (such as soil thickness and slope) in the triggering process. With respect to the case study described in this paper, starting from field evidences, further experimental tests should be performed, also considering the other soil types outcropping on Monte Mario. In this way, it will also be possible to verify if the current inferences may be extended to the entire area. In this fashion, physical laboratory modelling can also be viewed as a supporting tool for numerical models aimed at temporal and spatial prediction of shallow landslides occurrence over large areas. In fact, the rationale is to define the relation between rainfall, soil moisture, and triggering mechanisms for known laboratory boundary conditions and then to extend this relation at the investigated site through monitoring data collected in the field.

Data Availability

The data used to support the findings of this study are included within the article.

Conflicts of Interest

The authors declare that they have no conflicts of interest.

Acknowledgments

The authors thank two anonymous referees for their helpful suggestions and constructive comments, which have contributed greatly in improving the quality of the manuscript. The authors also thank the "Dipartimento per gli Affari Regionali e le Autonomie della Presidenza del Consiglio dei Ministri" for the financial support in the framework of the project "Grandi frane in roccia e frane superficiali a cinematica rapida in aree montane: metodi per la previsione temporale e spaziale (*prediction and susceptibility*)."

References

[1] F. C. Dai, C. F. Lee, and Y. Y. Ngai, "Landslide risk assessment and management: an overview," *Engineering Geology*, vol. 64, no. 1, pp. 65–87, 2002.

[2] C. W. Lin, S. H. Liu, S. Y. Lee, and C. C. Liu, "Impacts of the Chi-Chi earthquake on subsequent rainfall-induced landslides in central Taiwan," *Engineering Geology*, vol. 86, no. 2-3, pp. 87–101, 2006.

[3] M. Schwarz, F. Preti, F. Giadrossich, P. Lehmann, and D. Or, "Quantifying the role of vegetation in slope stability: a case study in Tuscany (Italy)," *Ecological Engineering*, vol. 36, no. 3, pp. 285–291, 2010.

[4] C. Camera, T. Apuani, and M. Masetti, "Modeling the stability of terraced slopes: an approach from Valtellina (Northern Italy)," *Environmental Earth Sciences*, vol. 74, no. 1, pp. 855–868, 2015.

[5] G. B. Crosta, P. Dal Negro, and P. Frattini, "Soil slips and debris flows on terraced slopes," *Natural Hazards and Earth System Sciences*, vol. 3, no. 1/2, pp. 31–42, 2003.

[6] M. G. Persichillo, M. Bordoni, M. Cavalli, S. Crema, and C. Meisina, "The role of human activities on sediment connectivity of shallow landslides," *Catena*, vol. 160, pp. 261–274, 2018.

[7] G. Formetta, V. Rago, G. Capparelli, R. Rigon, F. Muto, and P. Versace, "Integrated physically based system for modeling landslide susceptibility," *Procedia Earth and Planetary Science*, vol. 9, pp. 74–82, 2014.

[8] J. Y. Ho and K. T. Lee, "Performance evaluation of a physically based model for shallow landslide prediction," *Landslides*, vol. 14, no. 3, pp. 961–980, 2017.

[9] Z. Liao, Y. Hong, D. Kirschbaum, and C. Liu, "Assessment of shallow landslides from Hurricane Mitch in central America using a physically based model," *Environmental Earth Sciences*, vol. 66, no. 6, pp. 1697–1705, 2012.

[10] Y. Thiery, R. Vandromme, O. Maquaire, and S. Bernardie, "Landslide susceptibility assessment by EPBM (Expert Physically Based Model): strategy of calibration in complex environment," in *Advancing Culture of Living with Landslides*, M. Mikoš, Ž. Arbanas, Y. Yin, and K. Sassa, Eds., vol. 2017, Springer, Cham, 2017.

[11] R. I. Borja, X. Liu, and J. A. White, "Multiphysics hillslope processes triggering landslides," *Acta Geotechnica*, vol. 7, no. 4, pp. 261–269, 2012.

[12] K.-t. Chang, S.-. H. Chiang, and F. Lei, "Analysing the relationship between typhoon-triggered landslides and critical rainfall conditions," *Earth Surface Processes and Landforms*, vol. 33, no. 8, pp. 1261–1271, 2008.

[13] G. Sorbino and M. V. Nicotera, "Unsaturated soil mechanics in rainfall-induced flow landslides," *Engineering Geology*, vol. 165, pp. 105–132, 2013.

[14] R. L. Baum, J. W. Godt, and W. Z. Savage, "Estimating the timing and location of shallow rainfall-induced landslides using a model for transient, unsaturated infiltration," *Journal of Geophysical Research*, vol. 115, no. F3, 2010.

[15] A. W. Bishop, "The principle of effective stress," *Tek Ukebl*, vol. 106, pp. 859–863, 1959.

[16] J. W. Godt, R. L. Baum, and N. Lu, "Landsliding in partially saturated materials," *Geophysical Research Letters*, vol. 36, no. 2, 2009.

[17] D. G. Fredlund and H. Rahardjo, *Soil Mechanics for Unsaturated Soils*, John Wiley & Sons, Inc, New York, 1993.

[18] D. H. Kim, S. K. Kim, and I. Gratchev, "Unsaturated seepage behavior study using soil column test," *Proceedings of the 18th Southeast Asian Geotechnical Conference*, 2013, Singapore, 29-31 May, 2013, 2013.

[19] S. D. N. Lourenço, K. Sassa, and H. Fukuoka, "Failure process and hydrologic response of a two layer physical model: implications for rainfall-induced landslides," *Geomorphology*, vol. 73, no. 1-2, pp. 115–130, 2006.

[20] L. Montrasio and L. Schilirò, "Inferences on modeling rainfall-induced shallow landslides from experimental observations on stratified soils," *Italian Journal of Engineering Geology and Environment*, vol. 18, no. 2, pp. 77–85, 2018.

[21] L. Olivares and E. Damiano, "Post-failure mechanics of landslides: laboratory investigation of flowslides in pyroclastic soils," *Journal of Geotechnical and Geoenvironmental Engineering*, vol. 133, no. 1, pp. 51–62, 2007.

[22] G. Wang and K. Sassa, "Factors affecting rainfall-induced flowslides in laboratory flume tests," *Géotechnique*, vol. 51, no. 7, pp. 587–599, 2001.

[23] G. Wang and K. Sassa, "Pore-pressure generation and movement of rainfall-induced landslides: effects of grain size and fine-particle content," *Engineering Geology*, vol. 69, no. 1-2, pp. 109–125, 2003.

[24] L. Montrasio and R. Valentino, "Experimental analysis and modelling of shallow landslides," *Landslides*, vol. 4, no. 3, pp. 291–296, 2007.

[25] R. K. Regmi, K. Jung, H. Nakagawa, X. K. Do, and B. K. Mishra, "Numerical analysis of multiple slope failure due to rainfall: based on laboratory experiments," *Catena*, vol. 150, pp. 173–191, 2017.

[26] D. Tsutsumi and M. Fujita, "Relative importance of slope material properties and timing of rainfall for the occurrence of landslides," *International Journal of Erosion Control Engineering*, vol. 1, no. 2, pp. 79–89, 2008.

[27] N. Lu and W. J. Likos, *Unsaturated Soil Mechanics*, John Wiley & Sons, New York, NY, USA, 2004.

[28] N. Lu and J. Godt, "Infinite slope stability under steady unsaturated seepage conditions," *Water Resources Research*, vol. 44, no. 11, 2008.

[29] L. Montrasio, L. Schilirò, and A. Terrone, "Physical and numerical modelling of shallow landslides," *Landslides*, vol. 13, no. 5, pp. 873–883, 2016.

[30] T. van Asch, B. Yu, and W. Hu, "The development of a 1-D integrated hydro-mechanical model based on flume tests to unravel different hydrological triggering processes of debris flows," *Water*, vol. 10, no. 7, p. 950, 2018.

[31] H. An, T. T. Viet, G. Lee et al., "Development of time-variant landslide-prediction software considering three-dimensional subsurface unsaturated flow," *Environmental Modelling and Software*, vol. 85, pp. 172–183, 2016.

[32] M. Alvioli and R. L. Baum, "Parallelization of the TRIGRS model for rainfall-induced landslides using the message passing interface," *Environmental Modelling and Software*, vol. 81, pp. 122–135, 2016.

[33] R. L. Baum, W. Z. Savage, and J. W. Godt, "TRIGRS-A Fortran program for transient rainfall infiltration and grid-based regional slope stability analysis, version 2.0," in *U.S. Geological Survey Open-File Report, 2008–1159*, p. 75, Denver Publishing Service Center, Denver, CO, USA, 2008.

[34] R. Rigon, G. Bertoldi, and T. M. Over, "GEOtop: a distributed hydrological model with coupled water and energy budgets," *Journal of Hydrometeorology*, vol. 7, no. 3, pp. 371–388, 2006.

[35] J. Šimůnek, M. Huang, M. Šejna, and M. T. van Genuchten, *The HYDRUS-1D Software Package for Simulating the One-Dimensional Movement of Water, Heat, and Multiple Solutes in Variably-Saturated Media. Version 1*, International Ground Water Modeling Center, Colorado School of Mines, Golden, Colorado, 1998.

[36] R. Funiciello, G. Giordano, and M. Mattei, *Memorie Descrittive della Carta Geologica d'Italia*, vol. 80, Carta geologica di Roma, Roma, 2008.

[37] F. Bozzano, S. Martino, and M. Priori, "Natural and man-induced stress evolution of slopes: the Monte Mario hill in Rome," *Environmental Geology*, vol. 50, no. 4, pp. 505–524, 2006.

[38] D. Alessi, F. Bozzano, A. Di Lisa et al., "Geological risks in large cities: the landslides triggered in the city of Rome (Italy) by the rainfall of 31 January-2 February 2014. Italian Journal of Engineering Geology and," *Environment*, vol. 1, pp. 15–34, 2014.

[39] R. L. Baum, J. P. McKenna, J. W. Godt, E. L. Harp, and S. R. McMullen, "Hydrologic monitoring of landslide-prone coastal bluffs near Edmonds and Everett, Washington, 2001-2004," in *U.S. Geological Survey Open-File Report, 2005–1063*, p. 42, U.S. Geological Survey Publications Warehouse, 2005.

[40] M. Bordoni, C. Meisina, R. Valentino, N. Lu, M. Bittelli, and S. Chersich, "Hydrological factors affecting rainfall-induced shallow landslides: from the field monitoring to a simplified slope stability analysis," *Engineering Geology*, vol. 193, pp. 19–37, 2015.

[41] M. Bordoni, R. Valentino, C. Meisina, M. Bittelli, and S. Chersich, "A simplified approach to assess the soil saturation degree and stability of a representative slope affected by shallow landslides in Oltrepò Pavese (Italy)," *Geosciences*, vol. 8, no. 12, p. 472, 2018.

[42] P. D'Odorico, S. Fagherazzi, and R. Rigon, "Potential for landsliding: dependence on hyetograph characteristics," *Journal of Geophysical Research*, vol. 110, no. F1, article F01007, 2005.

[43] R. Schnellmann, M. Busslinger, H. R. Schneider, and H. Rahardjo, "Effect of rising water table in an unsaturated slope," *Engineering Geology*, vol. 114, no. 1-2, pp. 71–83, 2010.

[44] L. Claessens, G. B. M. Heuvelink, J. M. Schoorl, and A. Veldkamp, "DEM resolution effects on shallow landslide hazard and soil redistribution modelling," *Earth Surface Processes and Landforms*, vol. 30, no. 4, pp. 461–477, 2005.

[45] K. J. Shou and Y. L. Chen, "Spatial risk analysis of Li-shan landslide in Taiwan," *Engineering Geology*, vol. 80, no. 3-4, pp. 199–213, 2005.

[46] T. Uchida, K. Tamur, and K. Akiyama, "The role of grid cell size, flow routing algorithm and spatial variability of soil depth on shallow landslide prediction," in *5th International Conference on Debris-Flow Hazards Mitigation: Mechanics, Prediction and Assessment*, R. Genevois, D. L. Hamilton, and A. Prestininzi, Eds., vol. 2011, pp. 149–157, Casa Editrice Università La Sapienza, Rome, Italy, 2011.

[47] D. V. Griffiths, J. Huang, and G. A. Fenton, "Probabilistic infinite slope analysis," *Computers and Geotechnics*, vol. 38, no. 4, pp. 577–584, 2011.

[48] J.-C. Huang, S.-J. Kao, M.-L. Hsu, and J.-C. Lin, "Stochastic procedure to extract and to integrate landslide susceptibility maps: an example of mountainous watershed in Taiwan," *Natural Hazards and Earth System Sciences*, vol. 6, no. 5, pp. 803–815, 2006.

[49] J. Y. Ho, K. T. Lee, T. C. Chang, Z. Y. Wang, and Y. H. Liao, "Influences of spatial distribution of soil thickness on shallow landslide prediction," *Engineering Geology*, vol. 124, pp. 38–46, 2012.

[50] T. S. Nguyen, S. Likitlersuang, and A. Jotisankasa, "Influence of the spatial variability of the root cohesion on a slope-scale stability model: a case study of residual soil slope in Thailand," *Bulletin of Engineering Geology and the Environment*, pp. 1–15, 2018.

[51] G.-M. Saulnier, K. Beven, and C. Obled, "Including spatially variable effective soil depths in TOPMODEL," *Journal of Hydrology*, vol. 202, no. 1-4, pp. 158–172, 1997.

[52] F. Catani, S. Segoni, and G. Falorni, "An empirical geomorphology-based approach to the spatial prediction of soil thickness at catchment scale," *Water Resources Research*, vol. 46, no. 5, 2010.

[53] T. K. Tesfa, D. G. Tarboton, D. G. Chandler, and J. P. McNamara, "Modeling soil depth from topographic and land cover attributes," *Water Resources Research*, vol. 45, no. 10, 2009.

[54] M. T. van Genuchten, "A closed-form equation for predicting the hydraulic conductivity of unsaturated soils1," *Soil Science Society of America Journal*, vol. 44, no. 5, pp. 892–898, 1980.

[55] M. G. Schaap, F. J. Leij, and M. T. van Genuchten, "ROSETTA: a computer program for estimating soil hydraulic parameters with hierarchical pedotransfer functions," *Journal of Hydrology*, vol. 251, no. 3-4, pp. 163–176, 2001.

[56] D. T. Jensen, G. H. Hargreaves, B. Temesgen, and R. G. Allen, "Computation of ETo under nonideal conditions," *Journal of Irrigation and Drainage Engineering*, vol. 123, no. 5, pp. 394–400, 1997.